Scanning Microscopy

Volume 8 | Number 2 Article 6

6-12-1994

# Three-Dimensional Mapping of Mineral Densities in Carious Dentin: Theory and Method

J. H. Kinney
*Lawrence Livermore National Laboratory*

G. W. Marshall Jr.
*University of California*

S. J. Marshall
*University of California*

Follow this and additional works at: https://digitalcommons.usu.edu/microscopy

 Part of the Biology Commons

## Recommended Citation

Kinney, J. H.; Marshall, G. W. Jr.; and Marshall, S. J. (1994) "Three-Dimensional Mapping of Mineral Densities in Carious Dentin: Theory and Method," *Scanning Microscopy*: Vol. 8 : No. 2 , Article 6.
Available at: https://digitalcommons.usu.edu/microscopy/vol8/iss2/6

This Article is brought to you for free and open access by the Western Dairy Center at DigitalCommons@USU. It has been accepted for inclusion in Scanning Microscopy by an authorized administrator of DigitalCommons@USU. For more information, please contact digitalcommons@usu.edu.

Scanning Microscopy, Vol. 8, No. 2, 1994 (Pages 197-205) 0891-7035/94$5.00+.25
Scanning Microscopy International, Chicago (AMF O'Hare), IL 60666 USA

# THREE-DIMENSIONAL MAPPING OF MINERAL DENSITIES IN CARIOUS DENTIN: THEORY AND METHOD

J.H. Kinney*,[1], G.W. Marshall Jr.[2] and S.J. Marshall[2]

[1]Chemistry and Materials Sciences Department, Lawrence Livermore National Laboratory Livermore, CA 94550
[2]Department of Restorative Dentistry, University of California, San Francisco, CA 94143-0758

(Received for publication November 22, 1993 and in revised form June 12, 1994)

## Abstract

X-ray tomographic microscopy (XTM), a three-dimensional X-ray imaging technique, has been used to quantitatively map mineral concentrations in carious dentin. Data analysis from the XTM study indicates that variations in the mineral concentration surrounding the caries can be imaged in three dimensions with a spatial resolution that is sufficient to detect calcified and enlarged tubule spaces in the lesion. A three-dimensional image of the subsurface lesion indicates that lesion penetration is along the direction of the tubules. The mineral concentration in the uninfected dentin was measured by the XTM to be $1.29 \pm 0.14$ g/cm$^3$ based upon the tabulated X-ray attenuation coefficients for apatite. This value is in excellent agreement with averaged estimates for the mineral concentration in dentin (1.4 g/cm$^3$). Furthermore, the mineral concentration determined using XTM varies from 2.25 g/cm$^3$ in the remineralized dentin to as low as $0.55 \pm 0.17$ g/cm$^3$ in the demineralized tissue. The high concentration of mineral in the remineralized region suggests that organic matter is lost and mineral is deposited at some time during the caries process.

**Key Words**: Tomography, dentin caries, mineral concentration.

*Address for correspondence:
John H. Kinney
Lawrence Livermore National Laboratory
Chemistry and Material Science Dept.
Building 235, L356
Livermore, CA 94550
Telephone number: (510) 422-6669
FAX number: (510) 423-7040

## Introduction

Our understanding of the physiological and mechanical properties of calcified tissues benefits from accurate measurements of the spatial distribution of the mineral phases that comprise them. Variations in mineral concentration occur naturally, and are an inherent part of the structural components of these tissues [21]. In addition, microscopic and macroscopic variations in density occur with normal physiological changes and disease processes.

Dentin, which forms the internal hard tissue of teeth, is a calcified tissue consisting of three major microstructural features: tubules, intertubular dentin, and peritubular dentin [16]. The tubules are 1-3 $\mu$m in diameter and are partially filled by a highly mineralized region of peritubular dentin, about 1-2 $\mu$m in thickness. A less mineralized intertubular dentin fills the remaining volume around the tubules. The average composition of dentin is similar to that of bone—approximately 65 wt% calcium phosphate (apatite structure) and 35 wt% organic matter, mostly collagen, and water [2].

Dentin is subject to the common disease process, caries, which is associated with demineralization and, ultimately, collagen removal and cavitation. Under certain conditions, hypermineralization (brought about by reprecipitation of the mineral phase) occurs in areas surrounding the caries. Thus, the disease process associated with caries is superimposed on the natural structural fluctuations in mineral concentration.

Many techniques have been developed to measure variations in mineral concentration in calcified tissues. At the microstructural level, these techniques include optical microscopy (OM) [19], X-ray micro-radiography (MR) [7, 8], and backscattered scanning electron microscopy (BSEM) [3, 14, 15]. All of these techniques have drawbacks, particularly when used to study mineralization in dentin. Both OM and MR require thin sections, while BSEM requires polished surfaces. Thin sections and polished surfaces are difficult to prepare in dentin, and artifacts are introduced by the preparation [20]. Furthermore, although OM correlates changes in

birefringence to changes in mineral concentration, a quantitative relationship between mineral density and optical birefringence in dentin has not been established. Microradiography, though extremely sensitive to changes in mineral concentration, provides a through-thickness measure of the X-ray attenuation coefficient. The possibility of overlapping structures and non-planar surfaces makes quantitative measurements of the mineral density prone to error. Finally, the lack of good dentin standards makes BSEM difficult to quantify and to relate to compositional changes within dentin.

We have been developing a non-invasive procedure for accurately discriminating between naturally occurring variations in mineral concentration and the variations due to disease processes. This procedure, called X-ray tomographic microscopy (XTM), results in a quantitative, three-dimensional (3D) map of mineral distributions in hard tissues. It differs from other forms of microtomography in that the images are truly 3D, and the spatial resolution is microscopic [6]. XTM will allow us to follow changes in mineral concentration *in vitro*. It combines the high resolution advantages of the surface techniques and the quantitative aspects of the volumetric measurements without the artifacts caused by sample preparation [12].

## Materials and Methods

XTM uses monochromatic synchrotron radiation to measure the X-ray attenuation coefficient as a function of position in a sample with great precision. XTM is based on the same principles used in medical computed tomography (CT). The linear X-ray attenuation coefficient, $\alpha$, at a point $\mathbf{r}_{x,y,z}$ in a material is determined from a finite set of X-ray attenuation measurements (projection data) taken at different angles. The projection data (I) are the transmitted X-ray intensities reaching a position sensitive detector after passing through the sample. These data, which are directly related to the material's composition and microstructure, are given by

$$I = \int S(E)[\exp\{-\oint \alpha(x,y,z,E)dl\}dE] \qquad (1)$$

where S(E) is the energy spectrum of the X-ray source and $\alpha(x,y,z,E)$ is the energy dependent linear attenuation coefficient at a single point in the sample. The line integral is taken along a straight path dl through the sample. If the radiation can be made nearly monochromatic with photon energy $E_o$, the energy spectrum can be approximated by a delta function and eq. 1 reduces to the familiar form of the Radon transform [9]:

$$\ln(I_o/I) = \oint \alpha(x,y,z,E)dl \qquad (2)$$

Measurements of the attenuation through the sample as a function of angle are used to numerically invert eq. 2 to solve for $\alpha(x,y,z,E_o)$. From *a–priori* knowledge of the chemical composition of the sample, $\alpha$ can be used to provide a quantitative mapping of the mineral phases and their distributions.

The XTM system uses synchrotron radiation, a single crystal Si monochromator to select a single X-ray energy, a high resolution scintillator, and a charge coupled device (CCD) detector. The scintillator screen is a single crystal of $CdWO_4$ which is highly polished, and is coated with an anti-reflective compound to reduce blurring which might be caused by reflections from the surface. The visible light is projected onto the CCD using variable magnification optical lenses. These lenses were specially designed for a large field of view and high spatial resolution with minimal distortion.

A two-dimensional CCD array detector is used to convert the visible light from the scintillator into position sensitive electronic signals required for tomographic reconstruction. The CCD array allows the simultaneous collection of both multiple ray paths and multiple slices for a given orientation of the sample—thereby greatly speeding up the tomographic measurements. The CCD is cooled thermoelectrically to temperatures below -40°C to reduce dark current and readout noise. The optimal temperature for operation is CCD dependent, and must be established by making careful measurements of resolution and charge transfer efficiency. Finally, the CCD is read out as 12 bit data in a slow scan manner, thereby greatly reducing the noise and significantly increasing the linear range of the detector.

In practice, a sample is positioned on a goniometer that is mounted on a rotating stage. The goniometer allows the sample to be oriented such that, upon rotation, it does not precess out of the detector's field of view. The sample is initially translated out of the X-ray path, and an image is obtained of the incident X-ray beam. This reference image, taken without the sample, provides the values for $\mathbf{I}_o(x',y')$ in eq. 2. Next, the sample is placed between the X-ray path and the scintillator, and another image, the projection image, is acquired. The projection image provides the values for $\mathbf{I}(x',y')$ at a given angular orientation. The ratios of the logarithms of the reference image and the projection image provide values of the integrated attenuation along the individual ray paths. By rotating the sample in discrete angular increments through 180 degrees, enough data can be obtained to reconstruct the two-dimensional projection images into a three-dimensional image of the attenuation coefficients. This reconstruction procedure, known as reconstruction from projections, is performed by Fourier-filtered back-projection [4]. The time required to image a sample with half-degree rotational increments

through 180° is less than three minutes. An additional 25 minutes per sample is required to transfer the data from the detector to the computer with the present interface architecture. Reconstruction times, which are performed afterwards, take approximately one minute per slice on a Vax workstation. Because the reconstructions are performed "off-line", a large number of samples can be imaged in an eight-hour shift. With the faster interface that will soon be installed, the sample throughput is expected to double.

A model for dentin is assumed wherein the composition consists of a mineral phase and an organic phase (plus water). The X-ray mass attenuation coefficient of dentin, $\mu_d$, is given by the mass-weighted coefficients of the individual phases:

$$\mu_d(cm^{-2}\cdot g^{-1}) = w_m\mu_m + w_o\mu_o \qquad (3)$$

where $w_m$ and $w_o$ are the weighted fractions of the mineral and organic phases and $\mu_m$ and $\mu_o$ are the mass attenuation coefficients of the mineral and organic phases, respectively. XTM provides the measure of the linear attenuation coefficient, $\alpha$, which is related to $\mu_d$ through the relation:

$$\alpha_d = \rho_d\mu_d = (w_m\mu_m + w_o\mu_o)\,\rho_d \qquad (4)$$

where $\rho_d$ is the density of the dentin (2.2 g/cm$^3$).

The predominant mineral phase in dentin is an apatite structure based on hydroxyapatite or HA [$Ca_5(PO_4)_3OH$]. However, the demineralization-remineralization processes occurring near caries may alter this apatite structure. Some possible alternate mineral phases include fluorapatite or FA [$Ca_5(PO_4)_3F$], dicalcium phosphate dihydrate (DCPD or brushite) [$CaH(PO_4)\cdot 2H_2O$], and tricalcium phosphate (TCP or whitlockite) [$Ca_3(PO_4)_2$]. Table 1 lists these alternate mineral phases which may be present in caries along with their corresponding densities [10] and X-ray attenuation coefficients at 25 keV [17]. From the information in Table 1, it is apparent that XTM cannot easily distinguish between FA, TCP, and HA. However, the mineral concentration measured by XTM will be unaffected within the precision of the measurements because of the similar attenuation coefficients and densities among the phases. DCPD, however, will appear as a lower density phase with respect to HA because of its lower mass attenuation coefficient and density. Hence, in the absence of other measurements, large weight fractions of DCPD would provide misleading values of the mineral concentration within the caries. Fortunately, we believe that in dentin, DCPD is present (if at all) only in trace amounts. This is because TCP is more likely to precipitate in the presence of Mg ions than is DCPD [13].

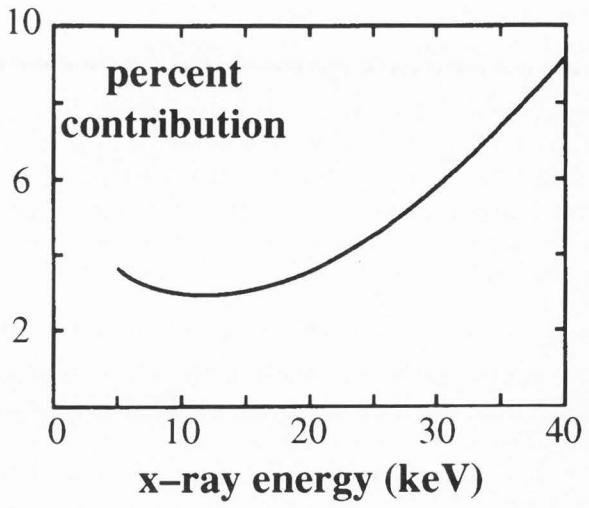


**Figure 1.** The percentage contribution of collagen to the total X-ray attenuation coefficient in natural dentin as a function of X-ray energy.

**Table 1.** X-ray mass attenuation coefficients at 25 keV for various mineral phases.

| Mineral phase | density (g/cm$^3$) | $\mu_m$ (cm$^2$/g) | $(\mu_m/\mu_{HA})$ |
|---|---|---|---|
| hydroxyapatite (HA) | 3.15 | 3.38 | 1.00 |
| fluorapatite (FA) | 3.2 | 3.37 | 0.99 |
| whitlockite (TCP) | 3.07 | 3.34 | 0.99 |
| brushite (DCPD) | 2.31 | 2.34 | 0.69 |

With an assumption for the organic phase, the concentration of the mineral phase in a caries lesion can be obtained with good accuracy from XTM data taken at a single energy. Dentin is approximately 35% by weight organic phase, which is primarily collagen. For calculating the collagen attenuation coefficient, we assume that collagen consists of glycine, proline, and hydroxyproline in a ratio of 30%, 40%, and 30% respectively [5]. With this model, collagen's contribution to the total X-ray attenuation coefficient in normal dentin is less than 5% at an X-ray energy of 25 keV. This percentage is shown in Figure 1 as a function of X-ray energy.

We assume that the collagen concentration, $C_o$, is invariant throughout the dentin, and has a value of 0.77 g/cm$^3$ (35 wt%). If the mass attenuation coefficient of the organic phase is given by $\mu_o$, then eq. 4 relates $\alpha_d$ to the mineral concentration, $C_m$, by

$$\rho_d\mu_d = \alpha_d = (C_m\mu_m + C_o\mu_o) \cong (C_m\mu_m + 0.77\mu_o)$$

$$C_m = [(\alpha_d - 0.28) / 3.38) \text{ (at 25 keV)} \qquad (5)$$

The effects of assuming that $C_o$ is constant throughout the caries can be estimated by considering the possible limits. Because the demineralization process is unlikely to enrich the matrix in collagen, the choice of a maximum value of the collagen concentration equal to the nominal concentration in unaffected dentin is reasonable. The lowest limit for the concentration would be zero. Using these limits, the true concentration of the mineral phase lies between

$$[(\alpha_d - 0.28) / 3.38) \leq C_m \leq (\alpha_d/3.38) \qquad (6)$$

The relative differences between the two assumptions range from near 10% in the demineralized zone to less than 3% in the remineralized dentin.

It is possible to separate the contributions from collagen and mineral phases in the analysis by performing XTM at two different energies [18]. Unlike dual energy CT using polychromatic radiation sources, the present analysis is simplified by the use of monochromatic radiation at two discrete energies. The linear attenuation coefficient at energies $E$ and $E'$ are given from eq. 5 as

$$\alpha_d(E) = \{C_m\mu_m(E) + C_o\mu_o(E)\}$$
$$\alpha_d(E') = \{C_m\mu_m(E') + C_o\mu_o(E')\} \qquad (7)$$

where the $\alpha_d$ have been determined at energies $E$ and $E'$, respectively. If XTM measurements are made at 20 keV($E$) and 25 keV($E'$), for example, then the mineral concentration can be determined without knowledge of the collagen using the relation

$$C_m = [\{\alpha_d(E) - 1.47\ \alpha_d(E')\} / 1.45] \qquad (8)$$

Equation 8 is obtained by solving eq. 7 simultaneously for $C_m$ and using tabulated values for $\mu_m$ and $\mu_o$ at the two different energies. Equations 5 and 8 are only valid within the accuracy of the tabulated X-ray attenuation coefficients used in this study. Using XTM to make more precise measurements of the mineral concentration will require absolute measurements of the attenuation coefficients for hydroxyapatite and collagen as a function of energy.

A maxillary cuspid with a natural caries lesion was used for the present study. The caries had advanced through the enamel layer and had attacked the dentin. No traces of the enamel remained. A 3 mm by 1 mm section was removed from the tooth using a standard Isomet saw. This section was stored in distilled water with 0.02% thymol until imaged.

The section was removed from the solution and mounted to a goniometer in the XTM apparatus. The sample was imaged in air using 25 keV synchrotron radiation at the 15-period wiggler beamline 10-2 at Stanford Synchrotron Radiation Laboratory [11]. A Si (220) reflection was used to make the beam nearly monochromatic to better than $\pm$ 25 eV. The energy was calibrated to the silver k-edge at 25.5 keV. Half degree rotational increments were used to obtain the necessary number of projection images to reconstruct the three-dimensional image.

The use of synchrotron radiation for this study was dictated by the desire to quantify the mineral density. The high intensity of the synchrotron source makes it practical to use monochromators to select a single wavelength. Thus, the attenuation coefficients that are measured with synchrotron radiation do not have to be corrected for polychromatic aberrations, the so-called "beam hardening" effects.

## Results

Figure 2a is a through thickness digital radiograph of the specimen taken using monochromatic synchrotron radiation at 25 keV. The large sample thickness ($\sim$ 1 mm) contains too many overlapping and non-planar structures to show much detail in the lesion. Figure 2b is an XTM section from the same sample, approximately 130 $\mu$m in from the front surface. The XTM section is 6.5 $\mu$m thick, and the reduction in the thickness from the radiograph allows greatly enhanced contrast of the mineral variations. Important differences exist between the two images. Figure 2a, the digital radiograph, shows the transmitted X-ray intensity reaching the detector. Hence, in Figure 2a, brighter regions correspond to lower attenuation (lower mineral concentration). The XTM images, on the other hand, depict the linear attenuation coefficient. In this case, brighter regions correspond to greater attenuation, hence, higher mineral concentration. Figures 2c and 2d are XTM images taken of sections lying parallel to the section in Figure 2b, but at 26 $\mu$m and 52 $\mu$m deeper into the sample, respectively. The differences between Figures 2b and 2d are significant. Because of this, through thickness measurements of natural caries in dentin can be affected by structural overlap even with 50 $\mu$m thick sections.

Figure 3 shows the mineral concentration along the line A-B in Figure 2b. The mineral concentration has been obtained from the XTM data using eq. 5. The surface of the sample has hypermineralized deposits, and exhibits mineral concentrations much greater than that found anywhere near the lesion ($> 2.5$ g/cm$^3$). The remineralized surface layer of the caries has a higher concentration than normal dentin. A rather abrupt gradient in mineral concentration outlines an interface between this remineralized zone and the surrounding normal dentin. The demineralized zone is penetrated by hypermineralized tubule spaces, indicating that ionic transport in dentin may be strongly influenced by the tubule network

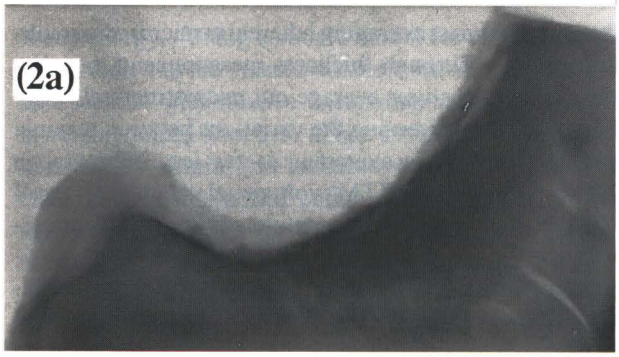


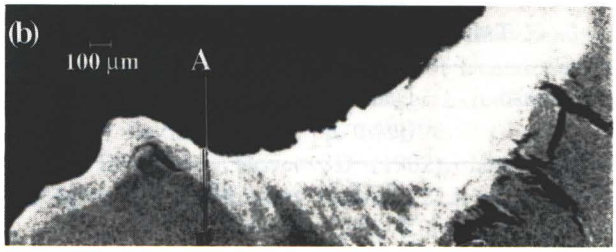


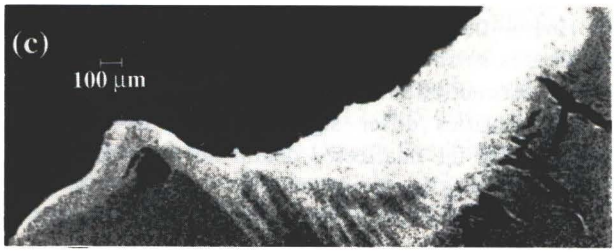



**Figure 2.** XTM images of a natural caries lesion. **(a)** The digital radiograph image through the thickness of the sample. **(b)** The XTM image of a single slice, 6.5 $\mu$m thick, taken approximately 130 $\mu$m inwards from the front surface. **(c)** XTM image of a slice parallel to the surface in Figure 2b but 26 $\mu$m farther into the sample. **(d)** XTM image of a single slice parallel to those in Figures 2b and 2c, but 52 $\mu$m farther into the sample. Bar = 100 $\mu$m.

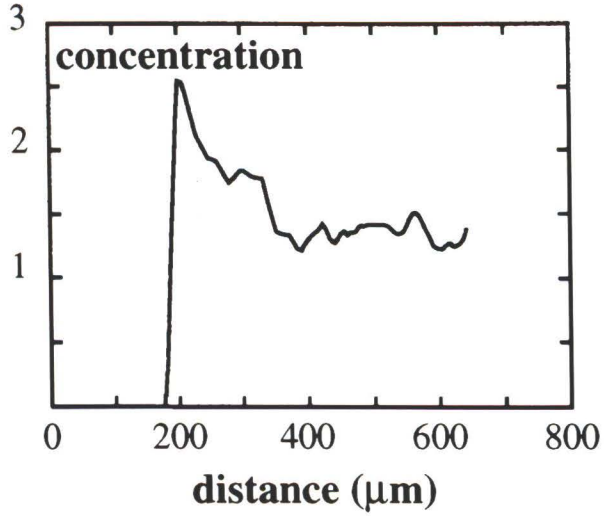


**Figure 3.** A line trace of the XTM data giving the mineral concentration (g/cm$^3$) along the path defined by the line A–B in Figure 2.

---

in a similar manner that microporosity is believed to affect mineral transport in enamel [19].

The lowest mineral concentration within the heart of the lesion is 0.55 $\pm$ 0.17 (g/cm$^3$) averaged over a cubic volume 25 $\mu$m on a side. The demineralized zone is surrounded by a partially remineralized zone containing a higher concentration of mineral phase than normal dentin. Immediately surrounding the demineralized zone, the mineral concentration increases rather abruptly

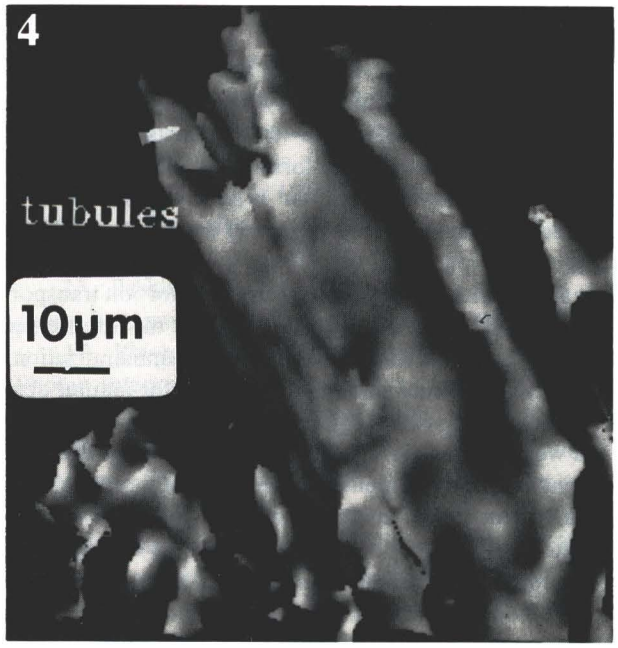


**Figure 4.** A three-dimensional rendering of a part of the demineralized lesion closest to the tooth surface showing etched-out tubules extending into the hypermineralized zone. The rendering is of the surface defined by a density contour of 1.2 g/cm$^3$. Bar = 10 $\mu$m.

**Table 2.** Standard model for dentin.

| Phase | Density ($g/cm^3$) | weight per cent | volume per cent |
|---|---|---|---|
| mineral | 3.15 | 65 | 45 |
| collagen | 1.6 | 35 | 48 |
| tubules | 0 | 0 | 7 |

to 1.61 $\pm$ 0.14 ($g/cm^3$). This hypermineralized zone, in turn, is surrounded by non-uniform regions of even higher concentration, ranging from 1.86 - 2.25 ($g/cm^3$). These densities differ significantly from the values measured in the unaffected dentin far from the lesion, 1.29 $\pm$ 0.14 ($g/cm^3$).

The XTM data are three-dimensional. Therefore, it is possible to visualize the true shape of the lesion. Figure 4 is a three-dimensional image of the subsurface lesion containing the volume occupied by material with density less than 1.2 $g/cm^3$. To obtain this image, we have rendered normal and hypermineralized dentin transparent in order to allow visualizing the subsurface demineralized regions. The main body of the lesion lies along the tubule direction. Enlarged tubule spaces can be seen in the perimeter of the lesion closest to the tooth surface. These spaces widen at the entrance to the lesion, since the peritubular dentin is demineralized first.

## Discussion

In the derivation of eqs. 5 and 8, it was assumed that dentin is composed entirely of mineral and organic phases. In reality, dentin *in vitro* consists of these two phases plus porosity in the form of tubules. The tubule volume fraction ranges from 1–22% depending upon position within the tooth and natural degree of variability within the population [16]. These tubules are fluid filled in natural dentin, and provide pathways for ion transport and bacterial invasion. In dentin caries, the tubules can become occluded with mineral during remineralization.

Table 2 defines our standard model for natural dentin based upon previously determined values for density and weight fractions. The XTM measurements are consistent with this model. According to this model, the volume fraction of mineral phase is 45%, the volume fraction of organic phase is 48%, and the tubules comprise roughly 7 vol% of the remaining tissue. The mineral concentration proposed in this model is in good agreement with the XTM data, but is 5% lower than that measured by Arends *et al.* [1] using microradiography. The difference in mineral concentration as determined by microradiography, and the values measured with XTM, may be due to natural variations in mineral concentration, the choice of attenuation coefficients, or a result of through-thickness averaging inherent in microradiographic imaging. Through thickness measurements of inhomogeneous structures average out microstructural variations, thereby decreasing the variations between maxima and minima. This averaging is far less important in XTM because the XTM volume elements are small enough to be more representative of the local composition.

In Arends' *in-vivo* study of dentin caries, no remineralization was observed. However, a mineral content of 25 vol% was observed in the demineralized zone, in fair agreement with the XTM results in the natural caries (18 vol%). Arends observed that the ultrastructural integrity was still intact in the demineralized dentin, and that this may be important for subsequent remineralization. If, during demineralization, the collagen remains unaltered, then the mineral content could increase during remineralization only by filling the remaining space. According to our model, mineral could occupy up to 52 vol% without altering the collagen. The maximum concentration of mineral according to this model, then, would be 1.64 $g/cm^3$. Indeed, this is close to what we observe in the remineralized region immediately adjacent to the demineralized zone.

XTM data from the most heavily remineralized regions, however, indicate that the mineral concentration is significantly greater than 1.6 $g/cm^3$. This can only come about through removal of collagen, indicating that at some stage in the caries development, collagen is removed from the dentin. Accounting for the large mineral concentrations observed in this study requires a reduction in the collagen, from 48 vol% to less than 40 vol%. A decrease in collagen of this amount most likely cannot be accounted for solely by the dissolution of the peritubular dentin, where tubule space enlargements of 30 percent and greater have been observed. Rather, intertubular dentin must demineralize as well. A possible model for dentin caries that explains the XTM observation consists of the demineralization and remineralization proceeding along the tubules at the outset, and expanding into the intertubular dentin after the peritubular dentin has been removed. The three-dimensional structure of the lesion indicates that demineralization is a complex phenomenon which is dependent upon the initial microstructural and microchemical variations in the dentin.

## Conclusions

XTM is a powerful three-dimensional imaging technique for mapping mineral density variations in large samples of calcified tissue. XTM does not require thin sectioning or fixing, and can be used for time-dependent studies *in vitro*. We have used XTM to map the mineral density variations surrounding a natural caries at a single

X-ray energy. Using a simple model for the dentin, the XTM data can be related to the concentration of hydroxyapatite with relative uncertainty ranging from 3% in remineralized tissue to about 10% in extremely demineralized dentin (the relative errors being due to uncertainty in the actual collagen concentration within the lesion). These model-dependent errors can be reduced by performing XTM at two different energies.

XTM was performed on a natural caries to demonstrate its potential for mapping out mineral density variations in calcified tissues. Mineral concentrations as low as 0.55 g/cm$^3$ (18 vol%) were measured in the heart of the demineralized zone. The remineralized portions of the lesion were found to contain as much as 2.25 g/cm$^3$ (71 vol%) mineral. This large concentration of mineral in the remineralized zone suggests that collagen was removed from the dentin at some point in the caries process.

Three-dimensional images facilitate our understanding of the shape, size, and growth directions of the lesion. In this example, lesion penetration is along the direction defined by the tubules, indicating that the tubules play an important role in the caries process in dentin. The ability to make *in vitro* measurements in three-dimensions will aid in determining the reaction rates and the dependence on pre-existing microstructure of demineralization processes in dentin. The application of XTM to mapping mineral variations in other calcified tissues is also envisioned.

## Acknowledgements

This work was funded by a grant from the National Institutes of Health/National Institute for Dental Research under P01DE09859. The work at Lawrence Livermore National Laboratory was conducted under the auspices of the U.S. Department of Energy under contract W-7405-ENG48. The synchrotron radiation was provided by the Stanford Synchrotron Radiation Laboratory which is funded by grants from DOE and NIH.

## References

1. Arends J, Ruben J, Jongebloed WL (1989). Dentine caries *in-vivo*. Caries Res **23**: 36-41.

2. Bhasicar SN (1990). Orban's Oral Histology and Embryology, 9th Edition, CB Mosby, St. Louis, MO.

3. Boyde A, Jones SJ (1983). Backscattered electron imaging of dental tissues. Anat Embryol **168**: 211-226.

4. Budinger TF, Gullberg GT, Huesman RH (1979). Emission computed tomography. In: Image Reconstruction from Projections-Implementation and Applications. Herman GT (ed.). Springer-Verlag, Berlin. pp. 190-200.

5. Butler WT, Richardson WS (1980). Biochemistry of tooth proteins. In: Biologic Basis of Dental Caries, An Oral Biology Textbook. Menaker L (ed.). Harper and Row, Baltimore, MD, pp. 168-190.

6. Elliott JC, Dover SD (1982). X-ray microtomography. J Microscopy **126**: 211-213.

7. Elliott JC, Dowker SEP, Knight RD (1981). Scanning X-ray microradiography of a section of a carious lesion in dental enamel. J Microscopy **123**: 89-92.

8. Featherstone JDB, Ten Cate JM, Shariati M, Arends J (1983). Comparison of artificial caries-like lesions by quantitative microradiography and microhardness profiles. Caries Res **17**: 385-391.

9. Herman GT (1980). Image Reconstruction from Projections: The Fundamentals of Computerized Tomography. Academic Press, New York.

10. Joint Committee for Powder Diffraction Standards, Powder Diffraction Data Base (Data on Calcium Phosphates) (1993). International Center for Diffraction Data, 1601 Park Lane, Swarthmore, PA 19081.

11. Kinney JH, Johnson QC, Nichols MC, Bonse U, Saroyan RA, Nusshardt R (1989). X-ray microtomography on Beamline 10 at SSRL. Rev Sci Instrum **60**: 2471-2474

12. Kinney JH, Nichols MC (1992). X-ray tomographic microscopy using synchrotron radiation. Annual Rev of Materials Science **22**: 121-152.

13. LeGeros RZ (1990). Chemical and crystallographic events in the caries process. J Dent Res 69: 567-574.

14. Marshall GW, Staninec M, Torii Y, Marshall SJ (1989). Comparison of backscattered scanning electron microscopy and microradiography of secondary caries. Scanning Microsc. **3**: 1043-1050.

15. Nelson DGA (1990). Backscattered electron imaging of partially demineralized enamel. Scanning Microsc. **4**: 31-42.

16. Pashley DH (1989). Dentin: A dynamic substrate — A review. Scanning Microsc. **3**: 161-176

17. Plechaty EF (1981). Tables and Graphs of Photon-Interaction Cross Sections. Lawrence Livermore National Laboratory Publication UCRL-50400 (available from the Technical Information Department, Lawrence Livermore National Laboratory, P.O. Box 808, Livermore, CA 94550).

18. Schneberk D, Martz H, Azevedo S (1991). Multiple-energy techniques in industrial computerized tomography. In: Review of Progress in Quantitative Nondestructive Evaluation, Vol. 10A. Thompson DO, Chimenti DE (eds.) Plenum, New York. pp. 451-456.

19. Silverstone LM (1970). Structure of carious enamel, including the early lesion. Oral Sci Rev **3**: 100-160.

20. Ten Cate JM, Nyvad B, Van de Plasshe-

Simons YM, Fejerskov O (1991). A quantitative-analysis of mineral loss and shrinkage of in-vitro demineralized human root surfaces. J Dent Res **70**: 1371-1374.

21. Weatherell JA, Robinson C, Hallsworth AS (1974). Variations in the chemical composition of human enamel. J Dent Res **54**: 180-192

## Discussion with Reviewers

**H.-J. Höhling and U.P. Wiesmann**: Will this paper be only a nice demonstration of the method of XTM or has such a X-ray microscopy laboratory the possibility for work on a caries project in detail?
**Authors**: Though this paper describes the technique of using the XTM to study dentin, we do not intend to leave it at that. We believe that a number of interesting questions regarding the distribution of mineral in teeth, the development of caries lesions, and mechanical failure of restorations can be cost-effectively studied with this method. At the present time, we are developing an *in vitro* caries cell that will allow us to study demineralization without desiccating the sample. XTM studies of mineralized tissues are ongoing in our laboratory. We plan to submit a paper on shrinkage accompanying demineralization of dentin shortly. Other studies involve laser treatment of dentin.

**H.-J. Höhling and U.P. Wiesmann**: Have you done XTM measurements with mineral and collagen standards to test assumptions of the model?
**J. Arends**: Has eq. 2 been checked with hydroxyapatite pressed pellets with known composition?
**Authors**: We are in the process of measuring the collagen and mineral standards to verify the assumptions of the model. In many other studies, however, we have found the differences between calculated cross-sections and measured values to be small (Kinney JH, Breunig TM, Starr TL *et al.* (1993) X-ray tomographic study of chemical vapor infiltration processing of ceramic composites. Science **260**: 789-792).

**H.-J. Höhling and U.P. Wiesmann**: Is it possible to carry out measurements on decalcified dentine to get an impression of the density of the organic matrix especially in the remineralized zone?
**Authors**: These studies are being performed currently. However, the matrix might be visualized in the demineralized zone, but would be obscured by the mineral in the remineralized zone.

**D.G.A. Nelson**: Can the technique be applied to enamel caries lesions?
**J. Arends**: Has the XTM technique applied to enamel? Is it possible to "visualize" enamel and dentin simultaneously?
**Authors**: Yes, the technique can be successfully applied to enamel and enamel caries lesions. Because the enamel contains less organic material, the interpretations of the results should be easier than with dentin. Simultaneously imaging dentin and enamel offers no problem.

**D.G.A. Nelson**: What is the spatial resolution of this technique and how thin can an XTM section be and contain useful information?
**Authors**: The ultimate resolution of the method is now between one to two micrometers in three-dimensions with an ability to detect high contrast features as small as 70 nm. However for this study, the voxel size was about 6 $\mu$m in order to image the entire sample. With slightly higher magnification, it was possible to image the etched tubules ($\sim$ 3 $\mu$m in diameter, see figure 4).

**K. Malmqvist**: You are working with monochromatic X-rays from SSRL for microtomographic studies of dentin. How would you compare this technique to another accelerator-based method, namely, ion microtomography making use of MeV light ions? In the ion technique higher depth resolution could be obtained, and in combination with PIXE (proton induced x-ray emission) elemental analysis, three dimensional reconstructions could be produced.
**Authors**: Ion microtomography (IMT) uses focused beams of protons (or other particles) with energies from 5 to 20 MeV. At 20 MeV, a proton beam would be able to penetrate about 3 mm of pure Ca, and perhaps somewhat less of dentin. Hence, IMT should just be able to look at a small section of dentin with good resolution. Because the contrast mechanism for IMT is somewhat different than that for X-ray absorption, the information content of the IMT images will provide additional data that would be of use for interpreting the chemical changes to dentin that occur with demineralization. The only drawback to IMT is the requirement for working in a vacuum.

PIXE is a powerful probe for elemental mapping; PIXE of thin specimens of dentin would be particularly useful in determining the concentration of mineral phase in the vicinity of the dentinal tubules. However, PIXE tomography might be possible on only very small samples because the fluorescent radiation from Ca and P has a very short mean free path in dentin.

**D.H. Pashley**: How do the authors know that the surface was covered with calculus rather than just hypermineralized deposits? Did they see bacteria in the calculus?
**Authors**: No we did not identify bacteria in these deposits.

**R.M.S. Schofield**: The method of determining the density of mineral fraction using two different X-ray energies seems potentially very sensitive to uncertainties in the mass attenuation coefficients because subtraction in the denominator of eq. 8 tends to amplify uncertainties. If accurate measurements of the attenuation coefficients were made on hydroxylapatite and collagen standards, roughly what magnitude of error would result from natural variations in composition between the specimens and the standards? Is the uncertainty in the water content of the specimen a concern in this method or in the single energy method you use here?

**Authors**: We included the discussion on dual energy techniques in order to emphasize that it is possible to use multiple energy techniques in order to extract quantitative information about materials containing multiple constituents. However, the difficulties in actually performing these measurements are precisely those mentioned by the reviewer; namely, small errors in the mass attenuation coefficients, or noise in the reconstructed data can greatly affect the calculated values. It is possible to obtain good experimental values of the attenuation coefficient of the mineral phase, but the organic phase is more problematic. Fortunately, the attenuation coefficient of the organic phase is small compared with the mineral phase, so that the effect on the measured concentrations will be small compared with the measured noise.

**R.M.S. Schofield**: Is there evidence indicating that the density of organic material does not increase in the demineralized zone as you assume for your estimate of the uncertainty in the mineral density?

**Authors**: There is indirect evidence that the density of the organic material does not increase in fully hydrated, demineralized dentin (Marshall *et al.*, Dent Mater **9**: 265-268, 1993). However, the collagen in fully demineralized dentin has been observed to shrink with drying. Therefore, careful measurements of the demineralization process should be made in solution.

**R.M.S. Schofield**: Could you go into a little more detail on some of the practical aspects of this technique? What is the maximum sample size and minimum spatial resolution for these specimens? What is the minimum reasonable time between extraction of the specimens and completion of data acquisition? Is desiccation a problem?

**Authors**: The maximum practical sample size is presently from one to two cm in cross-section. This limitation is presently dictated by the format of the charge coupled device detector. For accurate measurements of the attenuation coefficient, it is desirable that the sample remain in the field of view during rotation. If the CCD format size is 2000 pixel elements across the array, then a 2 cm diameter object can be imaged with a voxel size of 10 $\mu$m. In applications where the absolute attenuation coefficient is not required, for example simple imaging of structure, then the sample size is dictated by the ability of the X-rays to penetrate. In recent imaging of integrated circuits we find that the resolution is about 2 $\mu$m (voxel sampling size of 1 $\mu$m) and high contrast features as small as 70 nm can be detected. A minimum reasonable time between extraction and acquisition is one day. Since the data acquisition requires at most one hour, most of the delay is associated with the logistics of delivering the extracted tooth to the synchrotron source. Desiccation is not a problem, as the samples can be stored and imaged in solution.